Conf-9010185--19

IRRADIATION-INDUCED SENSITIZATION OF AUSTENITIC STAINLESS STEEL IN-CORE COMPONENTS*

CONF-9010185--19

DE91 006454

by

H. M. Chung, J. E. Sanecki, W. E. Ruther, and T. F. Kassner

Materials and Components Technology Division
Argonne National Laboratory
Argonne, Illinois 60439

October 1990

DISCLAIMER

Presented at the Eighteenth Water Reactor Safety Information Meeting, October 22-24, 1990, Rockville, MD.

*Work supported by the Office of Nuclear Regulatory Research, U. S. Nuclear Regulatory Commission.

IRRADIATION-INDUCED SENSITIZATION OF AUSTENITIC STAINLESS STEEL IN-CORE COMPONENTS

H. M. Chung, J. E. Sanecki, W. E. Ruther, and T. F. Kassner

Materials and Components Technology Division
Argonne National Laboratory
Argonne, Illinois 60439

Abstract

High- and commercial-purity specimens of Type 304 SS from BWR absorber rod tubes, irradiated during service to fluence levels of 6 x 10^{20} to 2 x 10^{21} n·cm^{-2} (E>1 MeV) in two reactors, were examined by Auger electron spectroscopy to characterize irradiation-induced grain boundary segregation and depletion of alloying and impurity elements, which have been associated with irradiation-assisted stress corrosion cracking (IASCC) of the steel. Ductile and intergranular fracture surfaces were produced by bending of hydrogen–charged specimens in the ultra-high vacuum of Auger microscope. The intergranular fracture surfaces in high-fluence commercial-purity material were characterized by relatively high levels of Si, P, and Ni segregation. An Auger energy peak at 59 eV indicated either segregation of an unidentified element or formation of an unidentified compound on the grain boundary. In contrast to the commercial-purity material, segregation of the impurity elements and intergranular failure in the high-purity material were negligible for a similar fluence level. However, grain boundary depletion of Cr was more significant in high-purity material than in commercial-purity material, which indicates that irradiation-induced segregation of impurity elements and depletion of alloying elements are interdependent.

1 Introduction

In recent years, failures of reactor–core internal components in both boiling- and pressurized-water reactors (BWRs and PWRs) have increased after accumulation of relatively high fluence (>5 x 10^{20} n·cm^{-2}, E > 1 MeV). The general pattern of the observed failures indicates that as nuclear plants age and the neutron fluence increases, a wide variety of apparently nonsensitized austenitic materials become susceptible to intergranular failure. Some of the failures have been reported for components that are subjected to a relatively low or negligible level of stress, e.g., control blade sheaths and handle and instrument dry tubes of BWRs. Although most failed components can be replaced, some safety-significant structural components, such as the BWR top guide, shroud, and core plate, would be very difficult or impractical to replace. Therefore, integrity of these structural components after accumulation of high fluence has been a subject of concern, and extensive research has been conducted to provide an understanding of this type of degradation process, commonly termed irradiation-assisted stress corrosion cracking (IASCC).[1-7]

Most of the safety-significant structural components are fabricated from solution-annealed austenitic stainless steels, primarily Type 304 stainless steel (SS), although Type

316 (Mo-modified), and 348 (Nb-modified) steels are also used. In addition, high-nickel alloys and Type 308 SS are also used in welding and joining the structural components. Component fabrication procedures and reactor operational parameters, such as neutron flux, fluence, temperature, water chemistry, and mechanical loads have been reported to influence susceptibility to IASCC. However, results from research at several laboratories on materials irradiated under a wide variety of conditions are often inconsistent and conflicting as to the influence of these parameters.[7] Failures of austenitic SS after accumulation of high fluence have been attributed to IASCC, in which irradiation-induced segregation or depletion of elements such as Si, P, S, Ni, and Cr at grain boundaries has been implicated. It is generally believed that the nonequilibrium process of radiation-induced segregation (RIS) of impurity or alloying elements is strongly influenced by irradiation temperature and fast-neutron dose rate. However, the identity of the elements that segregate and the extent to which RIS contributes to the enhanced susceptibility of the core-internal components of LWRs to IASCC are not clear.[7]

Characterization of RIS at grain boundaries of solution-annealed austenitic SS, irradiated in an LWR at temperatures near 300°C, has been conducted successfully only by means of Auger electron spectroscopy (AES)[4] and field-emission-gun scanning transmission electron microscopy (FEM-STEM).[5,6] Although results of such characterization have been reported recently for Type 348 SS after irradiation in a BWR[5], similar analysis of RIS in Type 304 SS from LWR field components has not been reported. In the present investigation, RIS in several specimens from two heats of Type 304 SS, obtained from control blade absorber tubes after service in two separate BWRs, has been analyzed by AES. One heat was a high-purity grade, and the other was commercial-purity. The objective of the investigation is to determine comparative characteristics of RIS in high- and commercial-purity heats of Type 304 SS that occur during service in BWRs. The microstructural modifications in the steels will be correlated with results of separate on-going tests in which susceptibilities of the two heats to stress corrosion cracking (SCC) are being measured in simulated BWR water.

2 Experimental Procedure

2.1 Materials and Irradiation

Type 304 SS was obtained from control blade absorber rod tubes that were irradiated in two BWRs. The absorber rods, containing B_4C absorber, were discharged from the reactors after several years of service. After removal of the B_4C by hammer-drilling, segments of the tubes were cut, cleaned, and notched to prepare specimens for analysis by AES. Chemical composition of the two heats of Type 304 SS from which the absorber tubes were fabricated is given in Table 1. In addition to irradiated specimens from these heats, unirradiated specimens, sectioned from a typical commercial heat of Type 304 SS that was used to fabricate other absorber tubes, were also analyzed to obtain baseline information on grain boundary microchemistry. The Type 304 SS irradiated in BWR-B was a high-purity (HP) grade, and the material irradiated in BWR-Y was a commercial-purity (CP) grade, Table 1. Beacuse documented composition of the CP material from the absorber tubes of BWR-Y was not available, a postirradiation chemical analysis was conducted. The Si content was found to be unusually high in the CP material, i.e., 1.55 wt%. In comparison, the Si content of the HP material was only 0.02 wt%. The fast-neutron fluence (E> 1 MeV) of the specimens is also given in Table 1.

Table 1. Chemical Compositions and Fluence of High- and Commercial-Purity Type 304 Stainless Steel BWR Absorber Rod Tubes Analyzed by Auger Electron Spectroscopy

Tube No.	Fluence (n/cm^2)	Reactor	Composition (in wt.%)									
			Cr	Ni	Mn	C	N	B	Si	P	S	O
ST-1	Nonirradiated	-	18.29	8.85	1.19	0.042	-	-	0.55	0.024	0.008	-
VH-A7A[a]	1.4×10^{21}	BWR-B	18.58	9.44	1.22	0.017	0.037	0.0002	0.02	0.002	0.003	-
BL-2H[b]	2.0×10^{21}	BWR-Y	16.80	8.77	1.65	-	0.052	-	1.55	-	-	0.024
BL-2M[b]	0.6×10^{21}	BWR-Y	16.80	8.77	1.65	-	0.052	-	1.55	-	-	0.024

[a]High-purity heat. Outer diameter and wall thickness are 4.78 and 0.63 mm, respectively. Chemical composition determined before irradiation.

[b]Commercial-purity heat. Outer diameter and wall thickness are 4.78 and 0.79 mm, respectively. Chemical composition determined after irradiation.

2.2 Auger Electron Spectroscopy

AES analyses were conducted with a JEOL Company JAMP-10 Model scanning Auger microscope (SAM). The instrument had a spatial-resolution capability of 50 nm and a depth resolution of one atomic layer. Notched specimens (0.8 x 3.0 x 20 mm) were electropolished in a solution of phosphoric-sulfuric acid (60:40 % by volume). Hydrogen charging was then conducted for 45 - 50 h in an electrolyte of 0.1N sulfuric acid with 100 mg/l of arsenic pentoxide or sodium arsenide, which act as a hydrogen recombination poisons. Following the hydrogen charging, some specimens were plated with cadmium or copper to minimize escape of dissolved hydrogen from the specimens. However, most of the specimens were fractured without plating of the surface. The hydrogen-charged specimens were transferred immediately to the ultra-high vacuum fracture chamber (2×10^{-9} torr) of the SAM, and fractured at room temperature. The freshly fractured surfaces were then examined in the spectrometer chamber of the SAM without being exposed to the atmosphere. Typically five to eight spots were selected for spectral analysis from regions of ductile and intergranular fracture. After the spectral analysis, depth profiles of alloying and impurity elements were obtained as a function of sputter distance beneath a selected region of intergranular fracture. The sputter removal rate was approximately 0.35 $nm \cdot s^{-1}$. Typically, an Auger spectrum was obtained after every 1-nm depth of sputter material was removed.

3 Results

3.1 Commercial-Purity Type 304 SS

The grain boundary microchemistry of several specimens from two axial positions of a CP absorber tube irradiated during service to fluence levels of 0.6 and 2×10^{21} $n \cdot cm^{-2}$ was analyzed. Figure 1 shows the morphologies of the fracture surfaces produced after hydrogen charging and in-situ fracture in the ultra-high vacuum of the SAM. Intergranular fracture was minimal (Fig. 1A) in the CP specimen irradiated to a relatively low fluence of 0.6×10^{21} $n \cdot cm^2$ (E>1 MeV), and predominantly ductile or transgranular cleavage was

Fig. 1. Morphologies of fracture surfaces produced in Type 304 SS absorber rod tubes after hydrogen charging and fracture in a scanning Auger microprobe at room temperature; (A) commercial-purity (CP) material irradiated in BWR-Y to a fluence of 0.6 x 10^{21} n·cm^{-2} (E > 1 MeV); (B) same as A, irradiated to a fluence of 2.0 x 10^{21} n·cm^{-2}.

observed. The composition of eight local spots (such as Spots 6 to 8) on the fracture surface of the low-fluence specimen was determined by AES. The results were consistent and reflected the bulk composition of the material. No indication of grain boundary depletion of Cr or segregation of impurity elements (Si, P, Cl) was detected. The only exception was the S-rich inclusions, which are denoted by Arrows 9 - 11 in Fig. 1A. No depth profiles were obtained on the low-fluence specimen because no clear intergranular fracture region could be discerned.

In contrast to the low-fluence CP specimen, the CP specimen irradiated to a fluence of 2.0 x 10^{21} n·cm^{-2} (E>1 MeV) showed a preponderance of intergranular separation (Fig. 1B). Auger electron spectra were obtained from a number of intergranular (e.g., Spot D, in Fig. 1B) and ductile (e.g., Spot F, in Fig. 1B) fracture regions of the specimen. Characteristic spectra (Fig. 2) were obtained from the intergranular and ductile regions of Fig. 1B, i.e., Spots D and F, respectively. Overall spectra, as well as magnified plots of the low-energy regions of the spectra, are shown in Figs. 2A (obtained from intergranular region) and 2B (ductile), and Figs. 2C (intergranular) and 2D (ductile), respectively, where the latter two better illustrate signals from impurity elements such as Si, P, and S. Comparison of spectra characteristic of intergranular and ductile fracture surfaces, such as those of Fig. 2, revealed the following: (1) signals from O, C, and S are caused by contamination from gases in the environment of the Auger microscope and the contamination was significantly greater on ductile fracture surfaces than on intergranular surfaces, and (2) signals corresponding to Ni, P, Si, and an unidentified energy peak at 59 eV were generally stronger for an intergranular fracture surface than for a ductile surface. To show these characteristics more quantitatively, Auger signals from several spots on ductile and intergranular fracture regions were analyzed, and peak-to-peak amplitudes of Ni, Cr, Si, P, and the 59-eV peak were measured and normalized with respect to the amplitude of the 701-eV peak of Fe.

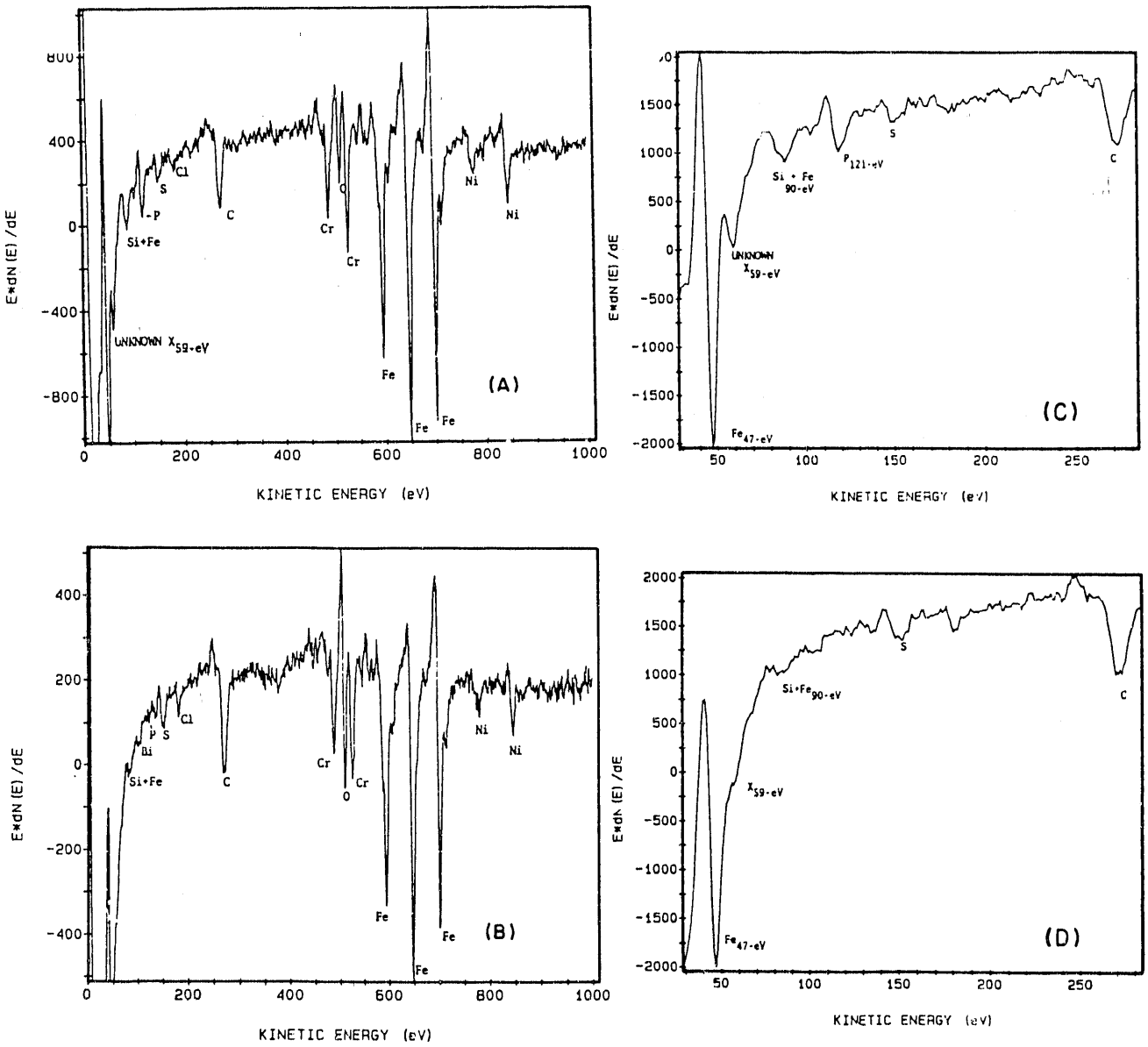

Fig. 2. Typical Auger spectra of (A) an intergranular fracture surface of CP Type 304 SS, from Spot D, Region 2, in Fig. 1B; (B) ductile fracture surface, from Spot F, Region 2, in Fig. 1B; (C) and (D) expanded spectra of A and B, respectively.

These normalized amplitudes, given in Table 2, correspond to the relative abundance of each element compared to the population of Fe atoms. In addition to the spectra obtained from five ductile and five intergranular fracture regions, three spectra were obtained from a faceted fracture surface of uncertain morphology. Although the latter morphology indicated a nonductile fracture of the local area, it was not clear if it could be attributed to grain boundary separation. However, the normalized amplitudes in Table 2 from intergranular fracture regions provide information on the relative concentration of elements on or near grain boundaries.

Table 2. Summary of Normalized[a] Peak-to-Peak Amplitudes of Auger Spectra of Several Alloying and Impurity Elements Obtained from Intergranular and Ductile Fracture Surfaces of Commercial-Purity High-Fluence Absorber Rod Tube (BL-2H, Table 1) after Hydrogen Charging

Location	Fracture Type[b]	Ni_{848-eV}	Cr_{526-eV}	$Si+Fe_{90-eV}$	P_{121-eV}	X_{59-eV}[c]
IC	D	255	435	60	23	2
2E	D	242	548	48	41	5
2F	D	230	436	48	36	11
5A	D	202	563	62	43	6
5C	D	244	538	73	21	1
1B	U	217	529	105	61	3
2A	U	229	626	83	13	12
2B	U	264	615	81	143	11
1A	I	321	519	145	118	84
2D	I	284	508	114	211	127
3A	I	322	544	110	183	106
5B	I	254	529	91	75	25
6A	I	315	541	125	206	78

[a]Normalized relative to the peak-to-peak amplitude of Fe_{701-eV}.
[b]D = ductile fracture, I = intergranular separation, U = uncertain faceted fracture surface morphology.
[c]Unidentified peak at ~59 eV.

The Auger peak near 90 eV is composed of adjacent signals of Si (91 eV) and Fe (88 eV). However, the contribution from 88-eV peak of Fe is relatively small, probably less than 3-5%,[4] which can be surmised from a comparison of the peaks shown in Figs. 2C and 2D. Therefore, the normalized amplitude denoted as $Si+Fe_{90-eV}$ in Table 2 should correspond primarily to Si concentration. The peak at 59 eV could not be identified. It is possible that the 61-eV Ni peak could shift both in energy and amplitude because of the formation of a thin film of a Ni-Si compound on the grain boundary. The 59-eV peak amplitude was proportional to both the amplitudes of the Ni and Si peaks; however, no conclusive identification could be made.

The normalized amplitudes, obtained for Ni, Si, P, and the unidentified 59-eV peak in Table 2, are plotted in Figs. 3-6, respectively. From these figures, the relative segregation of each element can be determined. Figure 3 shows that the Ni intensity tends to be higher on intergranular than on ductile fracture surfaces. Therefore, it can be concluded that Ni atoms segregate to grain boundaries where the concentration of Ni can be as much as 1.45 times greater than the bulk concentration. Silicon also became enriched at grain boundaries, by a factor of 3.5 above the bulk value (Fig. 4). Likewise, phosphorus also segregated

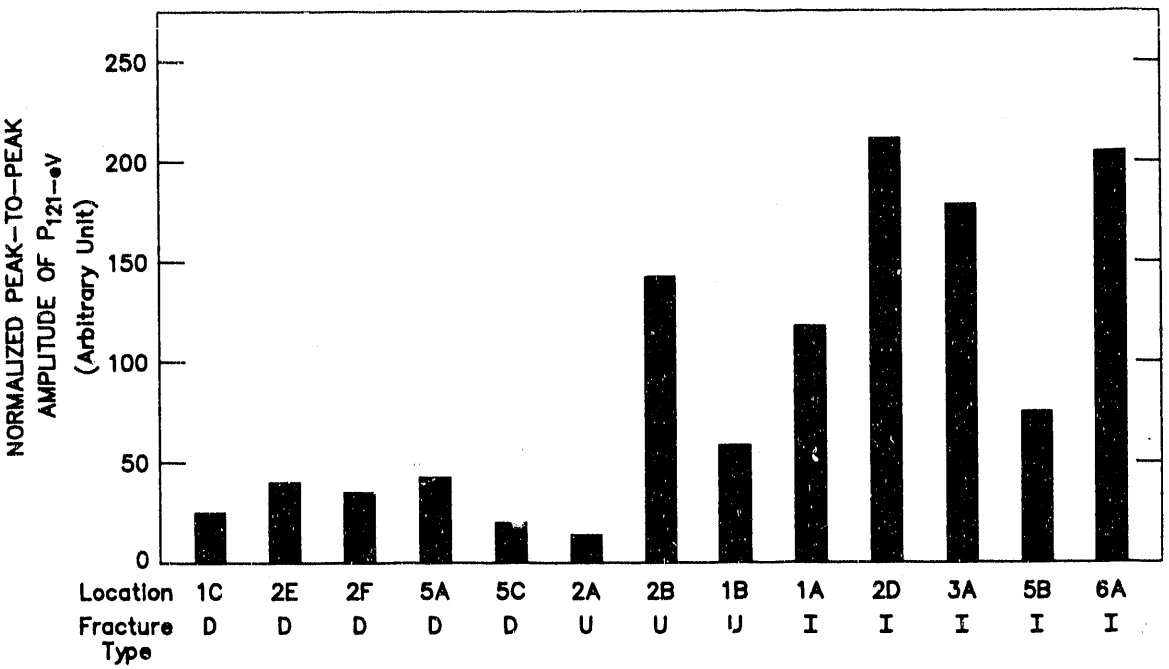

Fig. 5. Plot similar to Fig. 3 but obtained for P (121 eV).

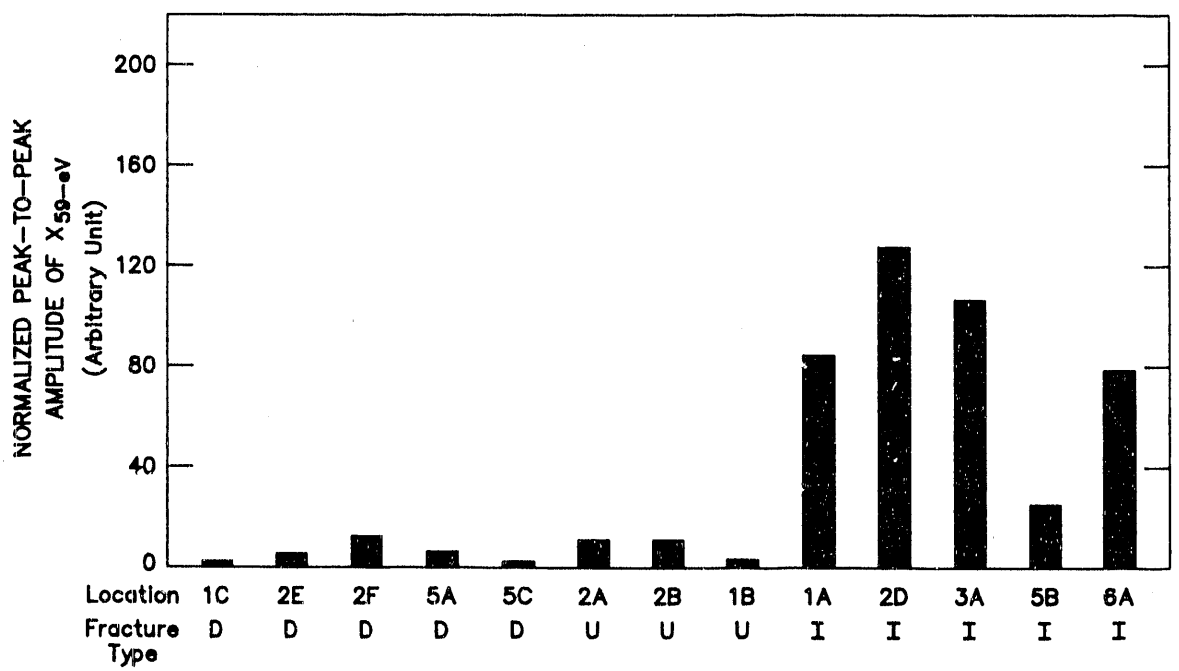

Fig. 6. Plot similar to Fig. 3 but obtained for an unidentified peak at 59 eV.

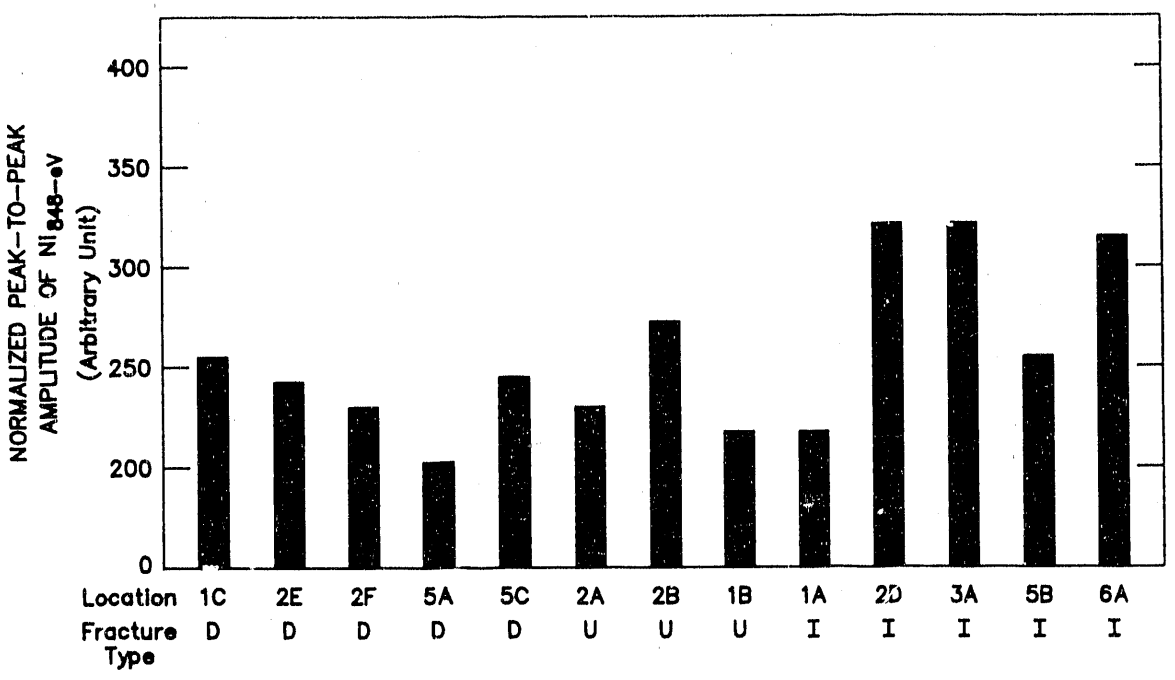

Fig. 3. Normalized peak-to-peak amplitude of Ni (848 eV) obtained from 13 locations on ductile (denoted by letter D), intergranular (I), and uncertain faceted (U) fracture surfaces of the CP absorber tube irradiated to 2.0 x 10^{21} n·cm^{-2} (E>1 MeV).

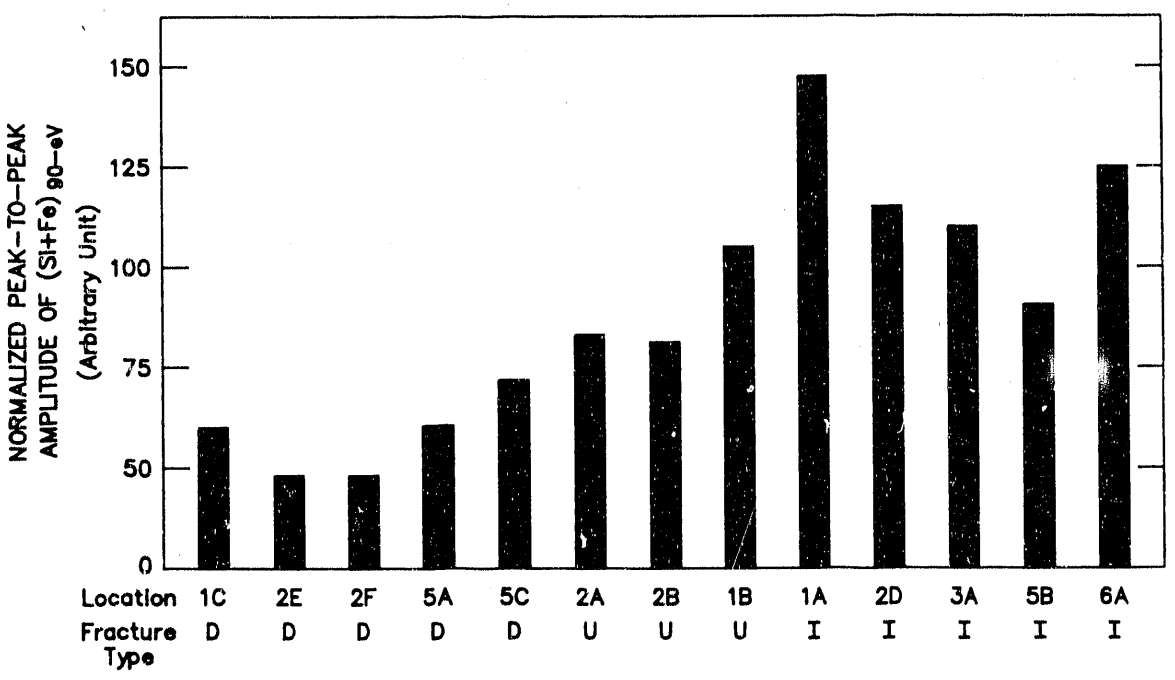

Fig. 4. Plot similar to Fig. 3 but obtained for Si (90 eV).

to grain boundaries where the levels are as much as nine times higher than the bulk concentration (Fig. 5). Although the 59-eV peak could not be identified at this time, Fig. 6 strongly indicates that intergranular fracture is associated with high intensity of this peak.

The distribution of Fe, Cr, and Ni could be characterized better by the depth-profile technique. The Fe, Cr, and Ni distributions in Fig. 7 were obtained by sputtering an intergranular fracture surface of the high-fluence CP Type 304 SS specimen. As expected, the grain boundary (denoted by the vertical dashed line in the figure) was depleted of Fe and Cr and enriched in Ni. However, the extent of Cr depletion was not significant in this specimen.

3.2 High-Purity Type 304 SS

Although the accumulated fluence (1.4×10^{21} n·cm^{-2}, E>1 MeV) and hydrogen-charging conditions for the HP specimen were similar to those of the CP specimens, it was difficult to produce intergranular fractures in the HP specimen. An example of a predominantly ductile fracture surface morphology is shown in Fig. 8A. Because of the lack of a clear intergranular fracture surface, it was not possible to obtain Auger spectra characteristic of a true grain boundary in this specimen. Consequently, another attempt was made to produce intergranular fractures in the high-fluence HP specimen by plating the specimen with Cu after hydrogen charging to increase retention of hydrogen in the specimen. Subsequent fracture of the Cu-plated specimen produced only limited intergranular separation beneath the outer surface of the tube. An example of the intergranular fracture surface is shown in Fig. 8B.

Analysis by AES was conducted on eleven intergranular, four ductile, and one uncertain cleavage-type fracture surfaces. However, in distinct contrast to the characteristics of the CP specimen of comparable fluence, no evidence of segregation of Si and P was observed. The intensity of the unidentified 59-eV peak was also negligible. Intensities of signals from S, C, and O were high, indicating significant contamination by adsorbed gases, as in the case of the CP specimens. In general, the intensity of the S peak was stronger than in the case of the CP specimens, which were fractured without the Cu-plating step. Apparently, higher sulphur contamination occurred during Cu plating because a sulphur-containing solution was used in the Cu-plating process. Thus, it was clear that no significant segregation of impurity elements occurred during irradiation of the HP specimens. However, a comparison of the normalized intensities of Ni obtained from the eleven intergranular and five other fracture surfaces showed that Ni became enriched at grain boundaries by a factor of 1.36 compared to the bulk concentration.

Figure 9 shows results of depth-profile analyses conducted on an intergranular fracture surface, i.e., Region 13 in Fig. 8B. In comparison with a similar result for the high-fluence CP specimen (Fig. 7), Fe and Cr depletion was more significant. The ratios for grain boundary depletion of Fe in the CP and HP specimens are 0.79 and 0.63, respectively. Corresponding ratios for Cr depletion for the CP and HP specimens are 0.88 and 0.40. In Figure 10, two profiles of the Cr depletion, obtained from the CP and HP specimens, are shown for comparison. The result shows a strikingly higher depletion of Cr for the HP specimen than for the CP specimen.

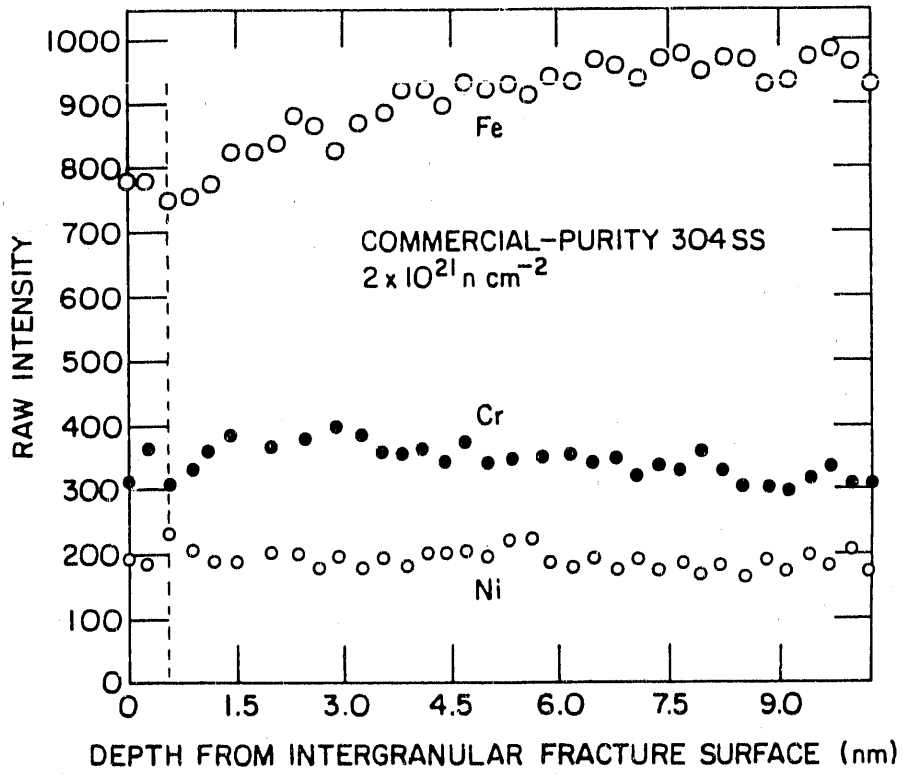

Fig. 7. Results of depth-profile analyses of Fe, Cr, and Ni obtained from an intergranular fracture surface similar to that shown in Fig. 1B.

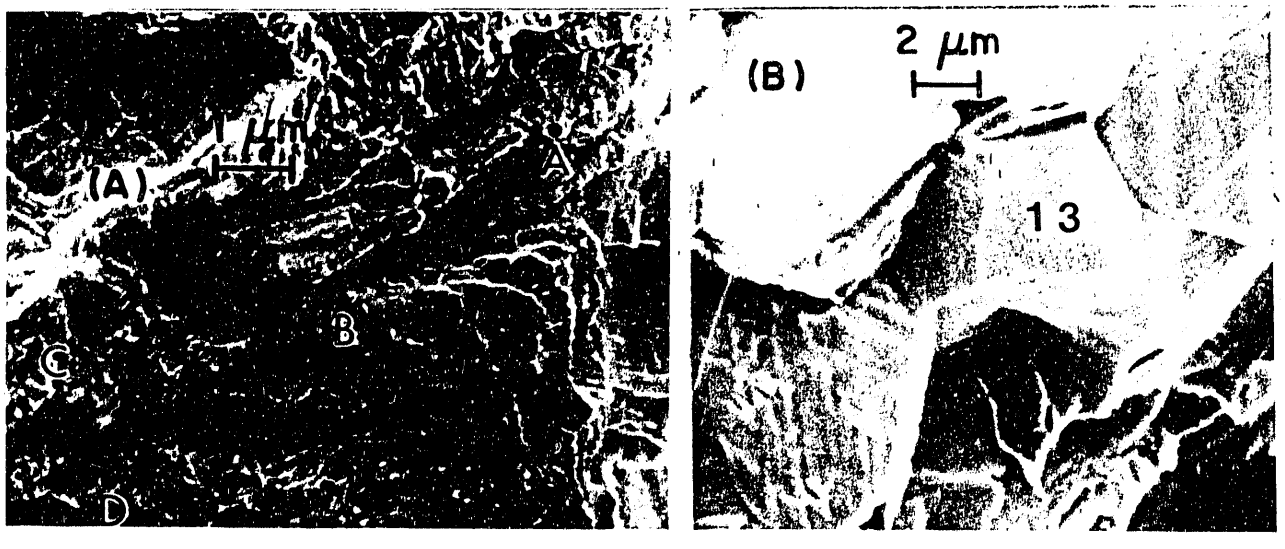

Fig. 8. Fracture surfaces of high-purity absorber tube irradiated to 1.4 x 10^{21} n·cm^{-2} (E > 1 MeV); (A) predominantly ductile fracture after hydrogen charging only; (B) intergranular fracture after hydrogen charging and Cu-plating.

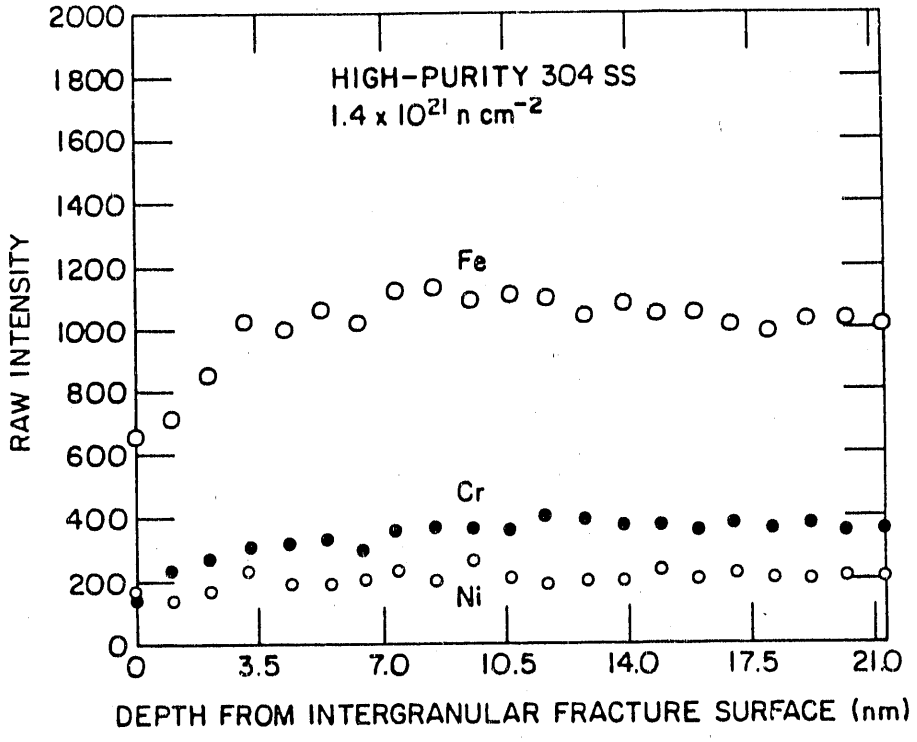

Fig. 9. Depth profiles similar to those shown in Fig. 7 but from the HP specimen irradiated to 1.4 x 10^{21} n·cm^{-2} (E > 1MeV), from Location 13, Fig. 8B.

4 Discussion

The AES analyses show that undersize atoms, namely, Si, P, and Ni, segregate to grain boundaries, whereas oversized atoms, namely Cr, diffuse away from grain boundaries. This is consistent with theory and experimental observations that have been reported previously.[4-6] Although grain boundary segregation of Si in Type 348 SS specimens has been well established from STEM analyses,[5,6] a previous AES[4] study on Type 304 SS irradiated in the Advanced Test Reactor (ATR) indicated that S was the major element that segregated to grain boundaries instead of Si or P. The latter elements were considered secondary impurities that segregated on intergranular fracture surfaces of the ATR-irradiated Type 304 SS. This is in direct contrast to the present results from the CP specimens, in which Si and P were the primary impurities that segregated. No evidence of S segregation was observed in the present study, although S, C, and O signals were attributed to contamination. For example, S intensities were consistently higher on ductile fracture surfaces than on intergranular fracture surfaces. Also, S contamination was particularly significant when the specimens were Cu-plated after hydrogen charging, implying a possible artifact effect. Sulfur should be detected by FEG-STEM; however, no evidence of S segregation was reported from such investigations on BWR-irradiated Type 348 or 304 SS. In view of this, the occurrence of S segregation and the role of S in IASCC of Type 304 SS in BWR environments is considered uncertain at best.

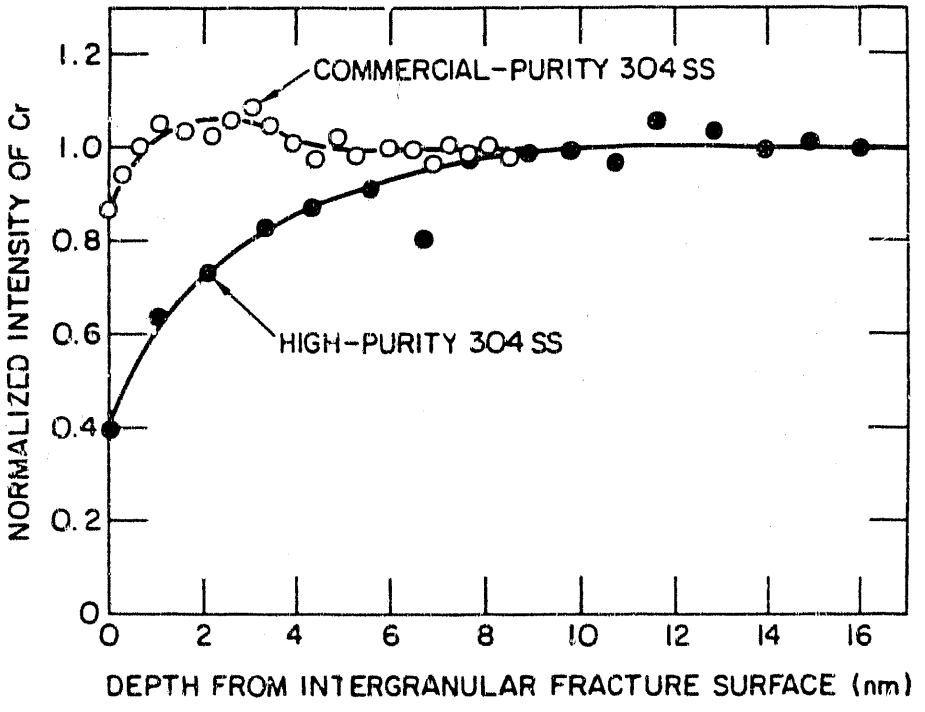

Fig. 10. Comparison of Cr-depletion profiles from intergranular fracture surfaces of high-fluence CP and HP materials shown in Figs. 7 and 9, respectively.

In contrast, intergranular fracture surfaces produced in the high-fluence CP specimens of Type 304 SS seem to be associated with significant segregation of Si, P, and the unidentified element or compound that gives rise to the 59-eV peak. This is particularly true in view of the insignificant Cr depletion in the CP specimens (Fig. 10). No clear correlation (similar to that of Si and P, in Figs. 4 and 5, respectively) could be established between intergranular failure and normalized Cr intensities for the CP specimens (Table 2). A synergistic interaction between Si and Ni enrichment on grain boundaries, which leads to formation of a thin film of G-phase (a phase rich in Ni and Si) or other Ni-Si compound, cannot be ruled out. A significant weakening of grain boundaries may occur as a result of such thin-film formation.

The absence of any significant segregation of impurity elements (except Ni) on grain boundaries of the HP specimens is obviously a result of the very low impurity content (Table 1). However, despite negligible impurity segregation, Cr depletion was more pronounced in the HP specimen than in the CP material for a similar fluence level. This suggests that there may be a synergism between Cr depletion and impurity segregation (i.e., less Cr depletion accompanying a pronounced impurity segregation). The two groups of oversized (Cr) and undersized (Si, P, and Ni) atoms diffuse in opposite directions, i.e., away from and toward a grain boundary sink, respectively. In this simultaneous process, Cr diffusion may be perturbed by the opposite flux of Si and P atoms, which thereby suppresses Cr depletion (e.g., in the CP material). Perturbation of Cr diffusion by the opposite flux of Ni may be negligible (e.g., in the HP material) because of negligible affinity between the two metallic elements.

The relative susceptibility of the CP and HP materials to SCC can be inferred from the characteristics of the irradiation-induced sensitization. If Cr depletion is the primary mechanism that controls SCC, HP specimens would be expected to exhibit a greater susceptibility to SCC than CP materials. If impurity segregation is the primary mechanism, an opposite result is expected. To clarify these contrasting alternatives to the IASCC process, slow-strain-rate tensile tests are being conducted in a hot-cell facility on specimens from the two heats of Type 304 SS in simulated BWR water.

5 Summary and Conclusions

1. Irradiation-induced sensitization in high- and commercial-purity Type 304 SS control blade absorber tubes, irradiated in two BWRs to a fast-neutron fluence of 2.0×10^{21} n·cm^{-2} (E > 1 MeV), has been characterized by Auger electron spectroscopy. Combined spectral and depth-profiling analyses yielded quantitative and qualitative information on grain boundary segregation and depletion of impurity and alloying elements.

2. Radiation-induced segregation of Si, P, Ni, and an unidentified element or compound that gives rise to an Auger energy peak at 59 eV was observed on grain boundaries of commercial-purity Type 304 SS after intergranular fracture of hydrogen-charged specimens. Such segregation was negligible in high-purity material, except for Ni. No evidence of S segregation was observed in either material.

3. Preliminary results indicate that Cr depletion from grain boundaries was more pronounced in the high-purity than in the commercial-purity material. This observation, coupled with the previous conclusion, suggests that a synergism occurs between impurity segregation and Cr depletion. SCC tests on the high- and commercial-purity steels are in progress to determine the relative importance of RIS of impurities and Cr depletion on intergranular fracture in simulated BWR water.

6 Acknowledgments

The authors are grateful to D. Donahue, G. Dragel, and R. A. Conner, Jr. for hot-cell operation and specimen preparation. The irradiated BWR components were obtained with the assistance of R. Kohli of Battelle Columbus Laboratory, A. J. Jacobs of General Electric Co., and J. L. Nelson of the Electric Power Research Institute. The authors are grateful to L. A. Neimark and W. J. Shack of Argonne National Laboratory and to J. Muscara of U. S. Nuclear Regulatory Commission for helpful discussions. This work was supported by the Office of Nuclear Regulatory Research, U. S. Nuclear Regulatory Commission.

7 References

1. W. L. Clark and A. J. Jacobs, *Effect of Radiation Environment on SCC of Austenitic Materials*, Proc. 1st Int'l. Symp. Environmental Degradation of Materials in Nuclear Power Systems - Water Reactors, National Association of Corrosion Engineers, 1984, pp. 451-461.

2. F. Garzarolli, D. Alter, and P. Dewes, *Deformability of Austenitic Stainless Steels and Ni-Base Alloys in the Core of a Boiling and Pressurized Water Reactor*, Proc. 2nd Int'l. Symp. Environmental Degradation of Materials in Nuclear Power Systems - Water Reactors, National Association of Corrosion Engineers, 1986, pp. 131-138.

3. F. Garzarolli, D. Alter, P. Dewes, and J. L. Nelson, *Deformability of Austenitic Steels and Ni-Base Alloys in the Core of a Boiling and a Pressurized Reactors*, Proc. 3rd Int'l. Symp. Environmental Degradation of Materials in Nuclear Power Systems - Water Reactors, The Metallurgical Society, Warrendale, Pennsylvania, 1987, pp. 888-999.

4. A. J. Jacobs, R. E. Clausing, L. Heatherly, and R. M. Kruger, *Irradiation Assisted Stress Corrosion Cracking and Grain Boundary Segregation in Heat Treated Type 304 Stainless Steel*, Effects of Radiation on Materials: 14th International Symposium, Vol. I, ASTM STP 1046, N. H. Packan, R. E. Stoller, and A. S. Kumar, eds., American Society for Testing and Materials, Philadelphia, 1989, pp. 424-436.

5. A. J. Jacobs, R. E. Clausing, M. K. Miller, and C. Shepherd, *Influence of Grain Boundary Composition on the IASCC Susceptibility of Type 348 Stainless Steel*, Proc. 4th Int'l. Symp. Environmental Degradation of Materials in Nuclear Power Systems - Water Reactors, Jekyll Island, Georgia, August 6-10, 1989, in press.

6. C. M. Shepherd and T. M. Williams, *Simulation of Microstructural Aspects of IASCC in Water Reactor Core Components*, ibid.

7. P. L. Andresen, F. P. Ford, S. M. Murphy, and J. M. Perks, *State of Knowledge of Radiation Effects on Environmental Cracking in Light Water Reactor Core Materials*, ibid.

END

DATE FILMED

01 / 31 / 91